Atmospheric
Chemistry
and Physics
Discussions

Open Access

EGU

1 **A set of methods to quantitatively evaluate the below-cloud evaporation**

2 **effect on precipitation isotopic composition: a case study in a city located**

3 **in the semi-arid regions of Chinese Loess Plateau**

4

5 Meng Xing[1,2*], Weiguo Liu[1,2,3*], Jing Hu[1,2]

6

7

8 1.State Key Laboratory of Loess and Quaternary Geology, Institute of Earth

9 Environment, Chinese Academy of Sciences, Xi'an, 710061, China

10 2.CAS Center for Excellence in Quaternary Science and Global Change，Xi'an,

11 710061, China.

12 3. University of Chinese Academy of Sciences, Beijing, 100049, China

13

14 Corresponding authors:

15 Meng Xing   email address: xingmeng@ieecas.cn

16 Weiguo Liu   email address: liuwg@loess.llqg.ac.cn

17

18
19
20
21
22
23
24
25
26
27
28
29
30

Atmospheric
Chemistry
and Physics
Discussions

31

32 Abstract:

33 Below-cloud evaporation effect heavily alters the initial precipitation isotopic

34 composition, especially in the arid and semi-arid regions, and leads to misinterpreting

35 the isotopic signal. To correctly explore the information contained in the precipitation

36 isotopes, the first step is to qualitatively analyze the falling raindrops encountered

37 below-cloud processes, and then to quantitatively compute the below-cloud

38 evaporation ratio of raindrops. Here, based on two-year precipitation and water vapor

39 isotopic observations in Xi'an, we systematically evaluated the variations of

40 precipitation and water vapor isotopes caused by the below-cloud evaporation effect.

41 Our results suggest that the equilibrium method could be successfully used to predict

42 the ground-level water vapor isotopic composition in semi-arid climates, especially for

43 the winter data. Moreover, by using $\triangle$d$\triangle$δ-diagram, our data showed that evaporation

44 is the mainly happened below-cloud process of raindrops, while snowfall samples

45 retained the initial cloud signal because of less isotopic exchange between vapor and

46 solid phases. In terms of meteorological factors, both temperature, relative humidity,

47 and precipitation amount affect the intensity of below-cloud evaporation. In arid and

48 semi-arid regions, the below-cloud evaporation ratio computed by the mass

49 conservation equation would be overestimated relative to the isotopic method, while

50 relative humidity is the most sensitive parameter in computing the remaining fraction

51 of evaporation. In the Chinese Loess Plateau (CLP) city, raindrops are weakly

52 evaporated in autumn and winter, and heavily evaporated in spring and summer, and

53 in the meantime, the evaporation intensity is related to the local relative humidity. Our

54 work sets an integrated and effective method to evaluate the below-cloud evaporation

55 effect, and it will improve our understanding of the information contained in

56 precipitation isotopic signals.

57

58

59

60

61

62

63

64

65

Atmospheric
Chemistry
and Physics
Discussions

Open Access

EGU

1 Introduction

Hydrogen and oxygen isotopes of precipitation are the one of greatly important tools to trace the hydrological cycle and climate changes (Bowen et al., 2019; Gat, 1996). For the paleoenvironment, the isotopic signals of precipitation recorded in ice cores (Thompson et al., 2000; Yao et al., 1996), tree rings (Liu et al., 2004; Liu et al., 2017b), speleothems (Cai et al., 2010; Tan et al., 2014), and leaf wax of loess-paleosol deposits (Wang et al., 2018b) and lake sediments (Liu et al., 2017a, 2019) could be used to reconstruct the information of temperature, precipitation, and hydrological regimes in geologic history, as it had participated into the formation or growth of these geological archives. For the modern environment, the isotopic ratios of precipitation could be used to quantitatively constraint the water vapor contribution from advection (Peng et al., 2011), evaporation (Sun et al., 2020; Wang et al., 2016a), transpiration (Li et al., 2016a; Zhao et al., 2019), and even anthropogenic activities (Fiorella et al., 2018; Gorski et al., 2015), as precipitation itself is one of the most important parts of the water circulation processes. Due to the limitations from sampling and theory, however, there remains some uncertainty to decipher the information contained in precipitation by using hydrogen and oxygen isotopic ratios (Bowen et al., 2019; Yao et al., 2013).

Chinese Loess Plateau (CLP) is located in the arid and semi-arid areas, where the below-cloud evaporation and surface moisture evaporation effects on precipitation isotopes have been widely proved (Sun et al., 2020; Wan et al., 2018; Zhang and Wang, 2016), which means the information remained in precipitation isotopic composition may have been remodeled by the environmental factors. Therefore, before we utilize precipitation isotopes to reconstruct the climate changes or to trace the water vapor sources, we first need to have a set of reliable evaluation systems to diagnose whether the precipitation isotopic ratios have been distorted by the below-cloud evaporation effect. Second, we should quantitatively calculate the below-cloud evaporation ratio of precipitation. Lastly, we can be able to use the calibrated precipitation isotopes to discuss regional water vapor sources or global hydrological cycle after we exclude the below-cloud evaporation effect. But the present situation is that there is still a large gap in our understanding at the first and second steps, and hence further study is needed.

Over the past decades, to determine whether the hydrometeors have been evaporated during its falling, most studies depend on a second-order isotopic parameter (Jeelani et al., 2018; Li and Garzione, 2017), deuterium excess (defined as d-excess= δ^2H-

102    $8 \times \delta^{18}O$), which is the representative of the kinetic fractionations, since $^2H^1H^{16}O$

103   equilibrate faster than $^1H_2^{18}O$ in different phases (Clark and Fritz, 1997; Dansgaard,

104   1964). The lighter isotopes (^1H and ^{16}O) of raindrop are preferentially evaporated from

105   the liquid phase during its falling through unsaturated ambient air, which results in a

106   decrease of d-excess in rain. Accordingly, the d-excess in the surrounding water vapor

107   will increase. The slope of the local meteoric water line (LMWL) has also been widely

108   used as a metric to infer the below-cloud evaporation effect according to the theory of

109   water isotopic equilibrium fractionation (Chakraborty et al., 2016; Putman et al., 2019;

110   Wang et al., 2018a), in which the LMWL's slopes approximately equal to 8.0 belonging

111   to equilibrium fractionation and that is lower than 8.0 pointing to a non-equilibrium

112   fractionation, such as the re-evaporation of raindrops. Nonetheless, it should be noted

113   that a change of air masses, condensation in supersaturation conditions, and moisture

114   exchange in the cloud and sub-cloud layer also cause largely spatial variation in slopes

115   and d-excess values (Graf et al., 2019; Putman et al., 2019; Tian et al., 2018). As an

116   improvement, simultaneous observations of water vapor and precipitation are applied

117   to distinguish these processes and quantify below-cloud processes. Yu et al. (2015,

118   2016) used the custom-made sampling devices to collect daily water vapor samples

119   over the Tibetan and Pamir Plateau, and discussed moisture source impacts on the

120   precipitation isotopes. With the aid of the off-line water vapor sampling system,

121   Deshpande et al. (2010) analyzed the rain-vapor interaction using stable isotopes.

122   However, the old water vapor cryogenic trapping technique is time-consuming

123   (Christner et al., 2018), labor-intensive (Welp et al., 2012), and discrete (Wen et al.,

124   2016), limiting the further examination of the two-phase system.

125

126   In recent years, with the progress in optical laser systems, the relatively portable field-

127   deployable laser spectroscopic instruments, simultaneously measuring $^1H_2^{16}O$,

128    $^2H^1H^{16}O$, and $^1H_2^{18}O$ isotopes, allows performing online, autonomous, and long-term

129   site measurements of the water vapor stable isotopic composition (Aemisegger et al.,

130   2012; Christner et al., 2018). The emergence of this instrument exerts a great impact

131   on the study of water vapor isotopic composition, leading to a substantially increased

132   number of observations in near-ground water vapor, and deepens our knowledge in

133   water vapor isotopic variations and fractionation processes during the two-phase

134   transformation (Noone et al., 2011; Steen-Larsen et al., 2014). Wen et al. (2010) first

135   analyzed the d-excess$_{vap}$ (denotes the d-excess of water vapor) at hourly temporal

136   resolution in Beijing, China, and systematically discussed the controls on the isotopic

137   exchange between vapor and condensed phase. Griffis et al. (2016) used multi-years

138 water vapor and precipitation isotopic results to evaluate the water vapor contributions

139 to the planetary boundary layer from evaporation. Laskar et al. (2014) and Rangarajan

140 et al. (2017) comprehensively investigated the water vapor sources and raindrop-vapor

141 interaction in Taibei, and developed a box model to explain the controlling factors for

142 high and low d-excess$_{vap}$ events in this region. Combined with observations and

143 numerical simulations of stable isotopes in vapor and rain impacted by cold fronts,

144 Aemisegger et al. (2015) clearly revealed the importance of below-cloud processes for

145 improving the simulations. As a creative work, Graf et al. (2019) introduced a new

146 interpretive framework to directly separate the convoluted influences on the stable

147 isotopic composition of vapor and precipitation according to the theoretical

148 fractionation processes, especially the influences of equilibration and below-cloud

149 evaporation, which enables us to correctly figure out the governing below-cloud

150 processes in the course of a rainfall. Although Graf's et al. (2019) work gives us a new

151 guideline to more accurately judge the raindrops experienced below-cloud evaporation

152 effect, their work was only validated on a cold frontal rain event of short period, and

153 hence more works should be done to prove the general applicability of their framework.

154

155 On the other hand, to quantitatively calculate the below-cloud evaporation ratio of

156 raindrops, the falling raindrop model suggested by Stewart (1975) has been widely

157 used, as the raindrops experienced physical processes have been explicitly described

158 by this isotope-evaporation model (Müller et al., 2017; Sun et al., 2020; Zhao et al.,

159 2019). Based on Stewart's (1975) work, the remaining fraction of raindrop mass (F_r)

160 after evaporation could be calculated according to the difference of stable isotopic

161 ratios in collected precipitation near the ground and below the cloud base (See Data

162 and Methods, section 2.3.2, eq 7). We note that some of the studies used the mass

163 conservation model of a falling raindrop to calculate F_r (See Data and Methods, section

164 2.3.3, eq 8; Kong et al., 2013; Li et al., 2016; Sun et al., 2019; Wang et al., 2016b),

165 and some of the works assumed the F_r is a constant (Müller et al., 2017), but no work

166 has been reported by using ground-based and cloud-based observations of water

167 vapor isotopes to calculate the F_r according to our knowledge. Due to the numerous

168 uncertainty of the parameters in the mass conservation model, such as the factors of

169 terminal velocity, the evaporation intensity, and the diameter of the raindrops, the error

170 propagation will largely raise the deviation of F_r in the model. Furthermore, no work

171 has systematically evaluated the differences of F_r computed by the observed isotope

172 results and the classical mass conservation model, until now.

173

Atmospheric
Chemistry
and Physics
Discussions
Open Access

EGU

174 Here, we have measured the near-ground water vapor isotopic composition at a city
175 located in the CLP for 2 years, while collected 142 precipitation samples (including
176 snowfall samples). The objectives of this study are to: 1. test the applicability of the △
177 d△δ-diagram suggested by Graf et al. (2019) when it is used to diagnose the below-
178 cloud processes; 2. compare the differences of raindrops below-cloud evaporation
179 ratio calculated by the observed ground-based water vapor isotopic composition and
180 the mass conservation model; 3. understand the main meteorological factors, such as
181 temperature, relative humidity (RH), and precipitation amount, controlling on the
182 below-cloud evaporation effect, and the seasonal variations of below-cloud
183 evaporation ratio in CLP. With the advantages of the coupling observations of the
184 vapor and precipitation in stable isotopes near the ground level, this study will provide
185 a new set of methods to determine the below-cloud evaporation effect qualitatively,
186 and strengthen our insight into that effect in arid and semi-arid areas quantitatively.
187

188 **2 Data and methods**
189 **2.1 Sampling site**
190 As the capital city of Shaanxi province and the largest city in northwest China, Xi'an is
191 located on the Guanzhong Plain on the southern edge of the CLP at an average
192 elevation of 400 m. The city is located in a semi-arid to arid region and is representative
193 of most cities in the north and northwest of China (e.g., Lanzhou and Xining city, Fig.
194 1), while notable below-cloud evaporation effect has been reported by many studies in
195 this area (Sun et al., 2020; Wan et al., 2018; Zhu et al., 2016).
196
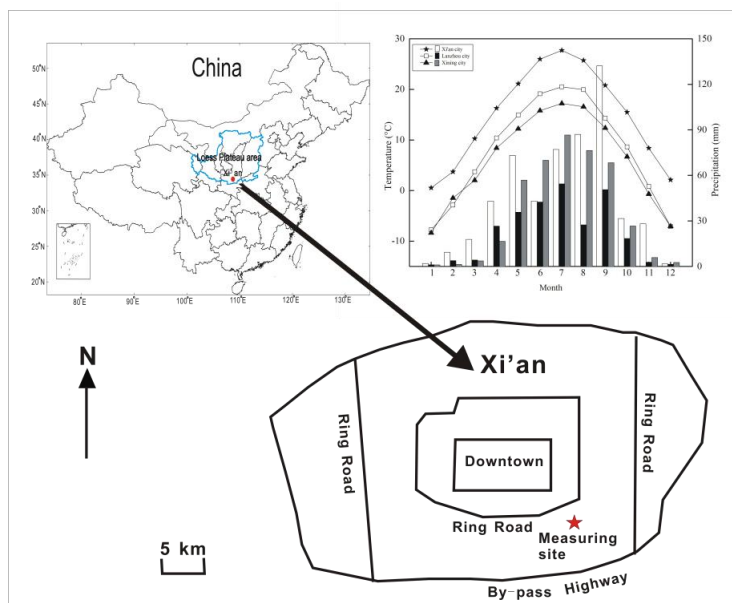197
198
199
200
201
202
203
204
205
206
207
208

Atmospheric
Chemistry
and Physics
Discussions

209
210

211 Figure 1 Average monthly variations of temperature and precipitation in Xi'an, Lanzhou, and
212 Xining during 2010-2015. Location of the sampling site in the Yanta Zone, 9 km SE of downtown
213 Xi'an. Water vapor samples are taken on the seventh floor of a twelve-story building, about 30
214 m above ground level. Precipitation samples are collected on the top floor, 1 m above ground
215 level.

216

217 The water vapor in-situ measurement is located in a residential area, approximately 10

218 km southeast to downtown of Xi'an city (Fig. 1). No specific pollution sources or point

219 sources are adjacent to the site. The atmospheric water vapor isotopic composition

220 was observed from 1 January 2016 to 31 December 2017 on the seventh floor of the

221 Institute of Earth and Environment, Chinese Academy of Sciences, about 30 m above

222 ground level. The rainfall or snowfall collector was placed on the rooftop of the

223 buildings (1 m above the floor of the roof).

224

225 **2.2 Sampling and isotopic measurement**

226 Rainfall and snowfall samples were collected manually from the beginning of each

227 precipitation event using a polyethylene collector (700 mm × 450 mm × 170 mm) and

228 the volume was measured using a graduated flask. Before being used, the collector

229 was cleaned with soap and water, rinsed with deionized water, and then dried. When

230 the precipitation events end, the collector was quickly taken back to minimize water

231 evaporation. Rainfall samples were immediately poured into a 100 ml polyethylene

232 bottle. The snowfall samples were melted at room temperature in a closed plastic bag

233 after collection, and then immediately poured into a 100 ml polyethylene bottle. After

Atmospheric
Chemistry
and Physics
Discussions
Open Access
EGU

234   collection, samples were filtered through 0.40–µm polycarbonate membranes. About

235   a 2 ml of each filtrate was transferred into a sample vial, and stored at – 4°C until being

236   measured. Of the 142 samples, during the two-year sampling campaign, we collected

237   131 rainfall and 11 snowfall samples (Table S1).

238

239   In all cases, the data are reported in the standard delta notation (δ), i.e., the per mil

240   (‰) deviation from Vienna Standard Mean Ocean Water according to, $\delta=$

241    $(R_{sample}/R_{reference}-1) \times 1000$, where R is the isotope ratio of the heavy and light isotope

242   (e.g., $^{18}O/^{16}O$) in the sample and the reference.

243

244   The precipitation samples were measured by Picarro L2130-i wavelength-scanned

245   cavity ring-down spectrometer at high-precision model, with the precision of better than

246   0.1‰ and 0.5‰ for $\delta^{18}O$ and δ^2H, respectively (Crosson, 2008; Gupta et al., 2009). All

247   the samples were calibrated by three laboratory standards, while the $\delta^{18}O$ and δ^2H true

248   values of the three laboratory standards (Laboratory Standard-1 (LS-1): $\delta^{18}O$ =+0.3‰,

249   δ^2H =–0.4‰; Laboratory Standard-2 (LS-2): $\delta^{18}O$ =–8.8‰, δ^2H =–64.8‰; Laboratory

250   Standard-3 (LS-3): $\delta^{18}O$ =–24.5‰, δ^2H =–189.1‰) are calibrated to the scale of two

251   international standard material VSMOW-GISP.

252

253   Atmospheric water vapor $\delta^{18}O_v$ and δ^2H_v were also measured by Picarro L2130-i, but

254   at a liquid-vapor dual model. The inlet of the gas-phase instrument is connected to the

255   vapor source through an external solenoid valve when measuring vapor samples. This

256   valve can switch the input of the instrument from the vapor sample to dry gas. The

257   instrument is connected to dry gas prior to being connected to the evaporator for

258   measuring liquid water standards so that any traces of the water vapor sample are

259   removed from the measurement cell. The standards are injected into the evaporator

260   and measured by a CTC Analytics autosampler, PAL HTC-xt (Leap Technologies,

261   Carrboro, NC, USA). The atmospheric water vapor is pumped through a stainless-steel

262   tube (1/8 inch) using a diaphragm pump and detected by the laser spectrometer.

263

264   The raw water vapor $\delta^{18}O_v$ and δ^2H_v data were obtained approximately at 1 Hz and

265   then block-averaged into 24 h intervals. As the main usage of this instrument is to

266   measure the liquid water samples in our laboratory, it is used to monitor the water

267   vapor isotopes in its spare time. Thus, the data gaps represent the instrument is in

268   liquid samples measuring status or maintenance.

269

Atmospheric
Chemistry
and Physics
Discussions

Open Access

EGU

270   The hourly meteorological data, such as temperature and RH in Xi'an, are reported by

271   the China meteorological administration, and can be downloaded from the websites of

272   http://www.weather.com.cn/. The meteorological station is about 10 km to the north of

273   our sampling site.

274

275   **2.3 Water vapor isotopic data calibration**

276   Due to the isotopic measurements of the cavity ringdown spectrometer with water

277   vapor concentration effect as outlined by some studies (Bastrikov et al., 2014; Benetti

278   et al., 2014; Steen-Larsen et al., 2013), it is important to determine the humidity-isotope

279   calibration response function. Because we did not have the Standards Delivery Module

280   (Picarro) system or equivalent, the humidity calibration is based on data obtained from

281   discrete injections of three known liquid standards with a PAL autosampler and the

282   Picarro vaporizer unit (Benetti et al., 2014; Noone et al., 2013). The analyzer is

283   programmed to perform a self-calibration after every 24 hours of ambient air

284   measurement using an autosampler to inject liquid standards for producing different

285   humidity. Injections were arranged at humidity levels near 3000, 5000, 8000, 10000,

286   15000, 20000, 25000 and 30000 ppm. Each reference sample is measured

287   continuously for 8 times at one humidity level, and the last 3 times results were used

288   to calculate the average to be recognized as the δ-value at the measured humidity.

289   The humidity correction is the difference between the δ-value at the measurement

290   humidity and the δ-value at a reference value taken as humidity = 20000 ppm. The

291   best fit was reached with an exponential function for $\delta^{18}O_v$ and a linear function for δ^2H_v

292   (Fig. S1a and S1b). The isotopic measurements of ambient air $\delta^{18}O_v$ samples were

293   corrected for humidity effects using:

294    $\delta^{18}O_{\text{humidity calibration}} = \delta^{18}O_{\text{measured}} - (-4.91 \times e^{(-3.51 \times \text{Measured humidity})})$ (eq 1)

295   and for ambient air δ^2H_v humidity correction using:

296    $\delta^2H_{\text{humidity calibration}} = \delta^2H_{\text{measured}} - (0.0001 \times \text{Measured humidity} - 1.86)$ (eq 2)

297   where $\delta_{\text{humidity calibration}}$ is the calibrated data for water vapor stable isotope; δ_{measured} is

298   the raw, measured data before calibration; and measured humidity is the

299   corresponding humidity at the time of measurement.

300

301   **2.4 Analytical methods**

302   **2.3.1 △d△δ-diagram**

303   As the raindrop falling from the cloud base to the ground, part of it will be evaporated

304   into the ambient atmosphere, however, it is very hard to quantify this process by

305   observation. Using stable water isotopes, Graf et al. (2019) introduced a △d△δ-

306 diagram to diagnose below-cloud processes and their effects on the isotopic

307 composition of vapor and rain since equilibration and evaporation are two various

308 below-cloud processes and lead to different directions in the two-dimensional phase

309 space of the $\triangle d \triangle \delta$-diagram. Here, the differences of isotopic composition ($\delta^{18}O_{pv-eq}$,

310 d-excess$_{pv-eq}$) of equilibrium vapor from precipitation samples relative to the observed

311 ground-based water vapor ($\delta^{18}O_{gr-v}$, d-excess$_{gr-v}$) can be expressed as:

312 $$\Delta\delta=\delta_{pv-eq} - \delta_{gr-v} \qquad\qquad (eq3)$$

313 $$\Delta\text{d-excess}_v=\text{d-excess}_{pv-eq} - \text{d-excess}_{gr-v} \qquad (eq4)$$

314 where δ_{pv-eq} and δ_{gr-v} are the δ^2H ($\delta^{18}O$) of water vapor below the cloud base and near

315 the ground, respectively, and d-excess$_{pv-eq}$ and d-excess$_{pv-eq}$ are d-excess values of

316 water vapor below the cloud base and near the ground, respectively.

317

318 To calculate the water vapor isotopic composition below the cloud base, we

319 hypothesize the constant exchange of water molecules between the liquid the vapor

320 phases during the falling of raindrop, and the isotopic compositions reach towards an

321 equilibrium in the two phases during the processes. In the equilibrium state, the

322 isotopic fractionation between the liquid and vapor phases follows a temperature-

323 dependent factor:

324 $$R_p=R_{pv-eq}\alpha \qquad\qquad (eq5)$$

325 where R_{pv-eq} is the water vapor isotope ratio between heavy and light isotopes ($^2H/^1H$

326 and $^{18}O/^{16}O$), R_p is the isotope ratio in precipitation, and α is a temperature-dependent

327 equilibrium fractionation factor. Here, when the temperature is greater than 0 °C, we

328 use the equation of Horita and Wesolowski (1994) to calculate $^2\alpha$ and $^{18}\alpha$, when the

329 temperature is below 0 °C, the equilibrium fractionation factor suggested by Ellehoj et

330 al. (2013) is considered.

331

332 The above equation can be converted into δ-notation as:

333 $$\frac{\delta_p}{1000}+1=\alpha(\frac{\delta_{pv-eq}}{1000}+1) \qquad\qquad (eq6)$$

334 where δ_p is the isotope ratio in precipitation.

335

336 **2.3.2 Below-cloud evaporation calculated by isotope**

337 Stewart (1975) suggested the falling raindrop isotopic fractionation of evaporation

338 could be calculated according to the fraction of raindrop mass remained after

339 evaporation:

Atmospheric
Chemistry
and Physics
Discussions

Open Access

EGU

$$\Delta\delta = \delta_p - \delta_{zp\text{-}eq} = (1 - \frac{\gamma}{\alpha})(F_{iso}^{\beta} - 1) \qquad (eq7)$$

where δ_p and $\delta_{zp\text{-}eq}$ are precipitation isotope ratio near the ground and below the cloud base, respectively; F_{iso} is the remaining fraction of raindrop mass after evaporation (hereafter, the remaining fraction of raindrop mass calculated by this method is denoted as F_{iso}); α is equilibrium fractionation factor for hydrogen and oxygen isotopes; the parameters of γ and β is defined by Stewart (1975). For the detailed calculation processes, please refer to the supplemental material (Appendix A), and Wang et al. (2016b), Sun et al. (2020), and Salamalikis (2016).

2.3.3 Below-cloud evaporation calculated by mass conservation model

Before the advent of the laser-based spectrometer, the method, which calculates the remaining fraction of raindrop mass according to the law of conservation of mass (hereafter, the remaining fraction of raindrop mass calculated by this method is denoted as $F_{raindrop}$), has been widely used (Kong et al., 2013; Li et al., 2016a; Sun et al., 2020; Wang et al., 2016b; Zhao et al., 2019):

$$F_{raindrop} = \frac{m_{end}}{m_{end} + m_{ev}} \qquad (eq8)$$

where the mass of the reaching ground raindrop without evaporation is m_{end} and the evaporated raindrop mass is m_{ev}. For the detailed calculation processes, please refer to the supplemental material (Appendix B), and Wang et al. (2016b), Sun et al. (2020), Kong et al. (2013), and Salamalikis (2016).

2.3.4 Statistical Analysis

To compare the difference of the below-cloud evaporation calculated by the two methods, the independent t-test was performed on SPSS 13.0 (SPSS Inc., Chicago, US). A significant statistical difference was set at $p < 0.05$.

**3 Results and discussion**

3.1 Relationship between water vapor and precipitation isotope ratios

In this study, the local meteoric water line (LMWL) is: $\delta^2H_p = 7.0 \times \delta^{18}O_p + 3.0$ based on event-based precipitation isotopic composition, and the local water vapor line (LWVL) is: $\delta^2H_v = 7.6 \times \delta^{18}O_v + 10.0$ based on daily water vapor isotopic composition (Fig. 2). Both the slope and intercept of LMWL are lower than that of Global Meteoric Water Line (GMWL), which are 8.0 and 10.0 (Dansgaard, 1964; Gat, 1996), respectively, indicating the potential for significant below-cloud evaporation effect on precipitation (Froehlich et al., 2008). In general, the slope of the meteoric water lines are indicative

375   of kinetic processes superimposed on the equilibrium fractionation, and the slope of

376   LWVL (slope=7.6) that shows a little lower than that of expected equilibrium

377   fractionation (slope=8.0) is also associated with the increasing influence of kinetic

378   processes (Rangarajan et al., 2017).
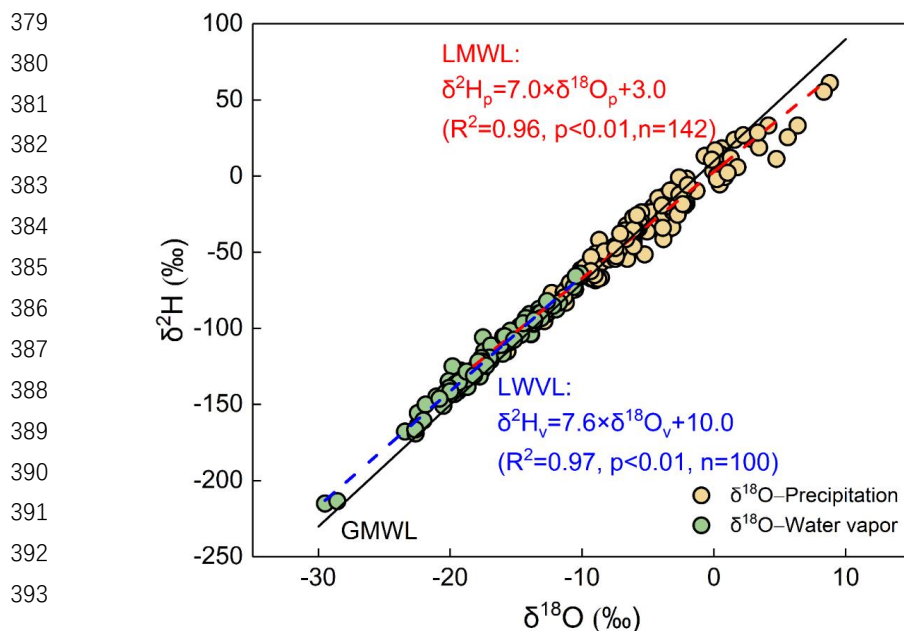
394   Figure 2 Local meteoric water line (LMWL) and Local water vapor line (LMVL) in Xi'an

395

396   Besides, we noted that the water vapor and precipitation isotopic composition basically

397   followed the same trend, and the water vapor isotopic composition is roughly more

398   negative than the precipitation isotopic composition (Fig. 2). According to the classical

399   isotopic fractionation theory, the heavier isotopes preferentially condense into the

400   liquid phase, and results in the precipitation isotopic ratios being more positive than

401   the corresponding water vapor isotopic composition during the precipitation process

402   (Dansgaard, 1964). Hence, the perfect distribution characteristics of water vapor and

403   precipitation on the $\delta^{18}O$-$\delta^{2}H$ plot would make us suppose that the precipitation isotopic

404   composition is mainly determined by its local water vapor isotopic composition in this

405   study site. To further validate our assumption, each of the event-based precipitation

406   isotopic ratio was plotted together with its water vapor isotopic composition of the

407   corresponding day, and they showed a significant positive correlation (Fig. 3a, R^2=0.66,

408   p<0.01). The water vapor isotopic composition can explain above 60% of the variation

409   of precipitation isotopic composition. Further, we used the measured precipitation

410   isotopic composition to deduce the water vapor isotopic composition at the cloud base

411   (1500m) according to the liquid-vapor equilibrium isotope fractionation, and compared

412   it with the observed near-ground water vapor isotopic composition. As expected, the

413   scatterplot of the observed $\delta^{18}O_v$ against the deduced $\delta^{18}O_{v\text{-}eq(1500m)}$ also presented a

414   significantly positive relationship, and the correlation coefficient increased a little as

415   well (Fig. 3b).
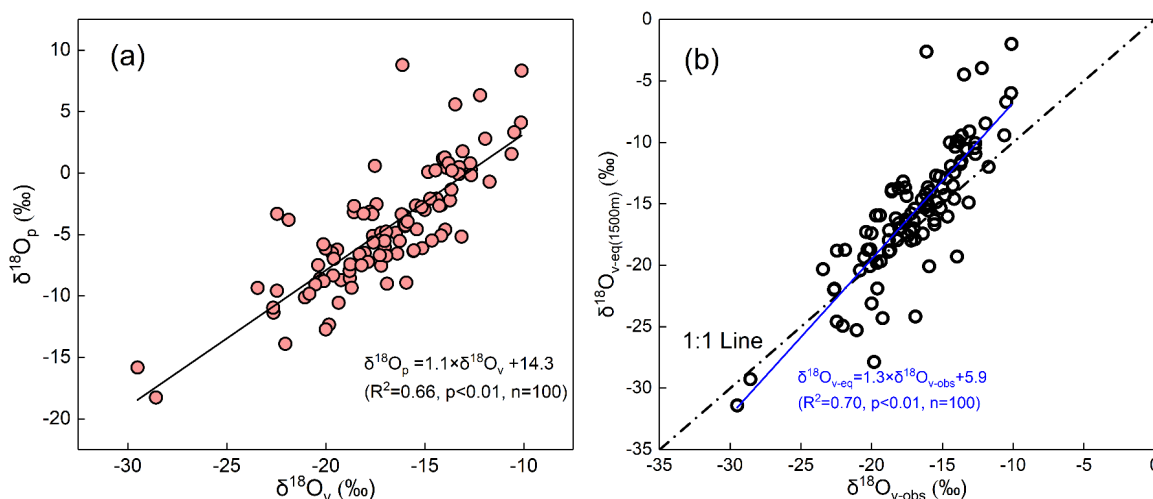
416   Figure 3 Relationship between $\delta^{18}O_p$ of precipitation and $\delta^{18}O_v$ of water vapor in Xian (a); and
417   relationship between the equilibrium computed 1500m $\delta^{18}O_v$ based on the precipitation isotopic
418   composition and the near ground observed $\delta^{18}O_v$ (b). The dash-dot line in (b) stands for the 1:1
419   line, and the blue line represents the regression line of the data.

420

421   The reasonable agreement of $\delta^{18}O$ between observed water vapor and equilibrium

422   prediction has been reported by Jacob and Sonntag (1991), Welp et al. (2008), and

423   Wen et al. (2010), however, they postulated the different relationship underlying the

424    $\delta^{18}O_v$ and $\delta^{18}O_{pv\text{-}eq}$. Jacob and Sonntag (1991) suggested that the water vapor isotopic

425   composition is possible to be deduced from the corresponding precipitation isotopic

426   composition, but Wen et al. (2010) pointed that the equilibrium method cannot

427   accurately predict the ground-level water vapor isotopic composition in arid and

428   semiarid climates. Here, our results indicate that it is possible to derive the isotope

429   composition of atmospheric water vapor based on that of the precipitation in the semi-

430   arid area.

431

432   In addition, we also noted that the equilibrium calculated $\delta^{18}O_{v\text{-}eq(1500m)}$ is relatively more

433   positive than the $\delta^{18}O_{v\text{-}obs}$ (Fig. 3b). Conventionally, the water vapor isotopic

434   composition decreases with the increase of altitude because of the decreasing

435   temperature (Deshpande et al., 2010; Salmon et al., 2019). However, due to the CLP

Atmospheric
Chemistry
and Physics
Discussions

Open Access

EGU

436 belonging to the semi-arid area, the raindrops are largely potential to be evaporated in

437 the unsaturated atmosphere during their falling as well as the $\delta^{18}O_p$ is subject to more

438 positive than its actual value. Therefore, the positively equilibrated $\delta^{18}O_{v-eq(1500m)}$ is

439 caused by the below-cloud evaporation effect, which makes the $\delta^{18}O_{v-eq}$-$\delta^{18}O_{v-obs}$ points

440 deviate from the 1:1 line. This reminds us that although the isotopic composition of

441 water vapor can be derived from the precipitation, the below-cloud evaporation effect

442 on altering the precipitation isotopic composition should be carefully noticed in the arid

443 and semi-arid area.

444

445 **3.2 Below-cloud processes indicated by $\triangle$d$\triangle$δ-diagram**

446 Traditionally, to qualitatively assess the below-cloud evaporation of raindrop, the value

447 of d-excess$_p$ is a benchmark, as the isotopically kinetic fractionation will cause d-

448 excess$_p$ deviate from 10‰, which is a theoretical value under vapor-liquid equilibrium

449 fractionation (Gat, 1996). Normally, below-cloud evaporation will move d-excess$_p$

450 below 10‰, and in comparison, mixing with the recycled water vapor from surface

451 evaporation and plant transpiration will bring d-excess$_p$ above 10‰ (Craig, 1961;

452 Dansgaard, 1964). However, considering the kinetic fractionation processes of

453 moisture transportation, the d-excess$_p$ information recorded in the collected

454 precipitation has been modified, and thus this enhances the uncertainty to gauge the

455 below-cloud evaporation process by solely using d-excess$_p$. Moreover, it is unable to

456 discern other below-cloud processes only based on d-excess$_p$. In contrast, the $\triangle$d and

457 $\triangle$δ diagram referred by Graf et al. (2019) provides richer information on the below-

458 cloud processes.

459

460 By projecting our data on the $\triangle$d and $\triangle$δ plot, the evaporation, equilibration, and non-

461 exchange processes could be clearly differentiated (Fig. 4). It is apparent from Fig. 4,

462 most of the precipitation samples are located in the fourth quadrant, indicating that

463 evaporation is the dominant below-cloud process. A small part of samples is distributed

464 in the first and second quadrant, and their $\triangle$δ are close to 0‰ while $\triangle$d are little higher

465 than 0‰. This cluster of samples implies that the below-cloud evaporation and cloud-

466 based isotopic fractionation tend to achieve a complete equilibrium state. Interestingly,

467 in our samples, most of the snow samples seize the third quadrant, which is suggestive

468 of below-cloud evaporation with less impact on them, and their initial signal after cloud-

469 based equilibrium fractionation is well retained. According to results from numerical

470 simulations and in-situ observations, Graf et al. (2019) summarized that raindrop size

471 and precipitation intensity appear to be the important driving factors of the below-cloud

472 processes, because raindrops with large diameter and high intensity will reduce its

473 residence time in the atmospheric column, and lower the evaporation possibility during

474 its way down toward the ground surface. However, as for snowfall events, it seems

475 unreasonable to explain the strongly negative $\triangle\delta$ from through the drop size and rain

476 rate (Fig. 4). It is well known that snowfall events generally happen in low-temperature

477 conditions, and corresponding to weak evaporation. Hence, rain/snow formed under

478 such circumstances, its isotopic signals will not be largely changed by the

479 environmental factors during its falling, which leads the $\triangle\delta$ to be more negative with

480 the decrease of temperature, such as the phenomenon observed in Graf's et al. (2019)

481 study during the post-frontal periods. Our results suggest that except for drop size and

482 rain rate, precipitation type is also an essential factor that needs to be fully considered

483 in the below-cloud processes.
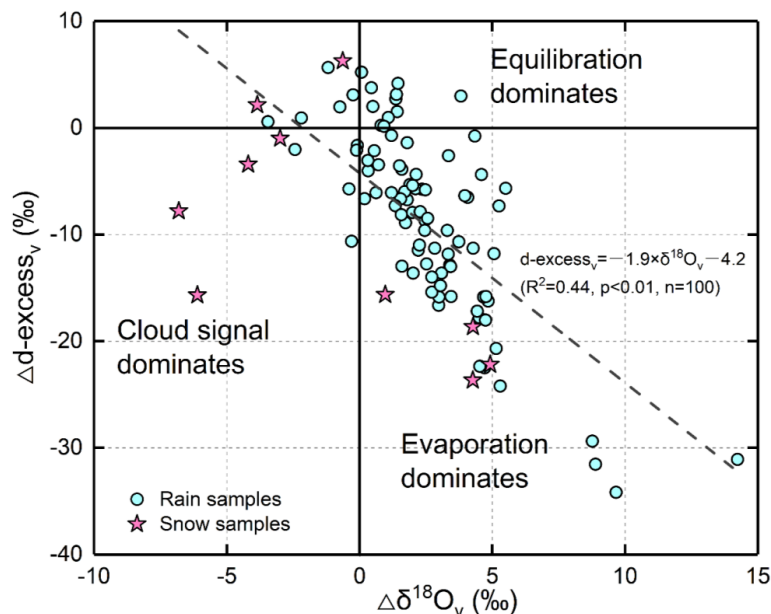
Figure 4 The projection of our data on Graf et al. (2019) suggested $\triangle d\triangle\delta$-diagram. The solid lines stand for $\triangle d\text{-excess}_v$ and $\triangle\delta^{18}O_v$ of 0‰. The dashed line corresponds to the linear fit through the samples.

503 Meteorological factors, such as precipitation amount, temperature, and RH, are the

504 main factors affecting below-cloud evaporation (Li et al., 2016b; Peng et al., 2007),

505 and have been well studied by combined with precipitation d-excess$_p$ (Ma et al., 2014;

506 Wang et al., 2016b). In order to further analyze the below-cloud processes, we added

Atmospheric
Chemistry
and Physics
Discussions
Open Access
EGU

507   the meteorological and isotopic information on the $\triangle d\triangle\delta$-diagram (Fig. 5). Generally,

508   with regard to high $\triangle^{18}O_v$ samples, the corresponding meteorological condition is high

509   temperature, low precipitation amount, and low RH (Fig. 5a-c). In contrast, under a

510   condition of low air temperature, high RH, and large precipitation amount, the $\triangle^{18}O_v$

511   of samples are relatively more negative (Fig. 5a-c). As below-cloud processes are

512   controlled by multi-variable factors, it is hard to only use one physical variable to

513   explain the below-cloud evaporation (Ma et al., 2014; Wang et al., 2016b). For example,

514   under the highest temperature condition (two most red dots in Fig. 5a), the below-cloud

515   evaporation effect should be higher, and cause $\triangle^{18}O_v$ to be more positive and $\triangle$d-

516   excess$_v$ to be more negative. However, under such circumstances, both the $\triangle^{18}O_v$ and

517     $\triangle$d-excess$_v$ of the two samples are close to 0‰. By considering the precipitation

518   amount, the two samples collected under the highest temperature condition are

519   associate with a relatively larger precipitation amount which will temper the intensity of

520   below-cloud evaporation. Similarly, the samples with lower precipitation amount is

521   associate with high RH, and cause the $\triangle^{18}O_v$ distributed around 3‰. For the snow

522   samples, the data with positive $\triangle^{18}O_v$ is regarding to the very low RH (Fig. 5c).
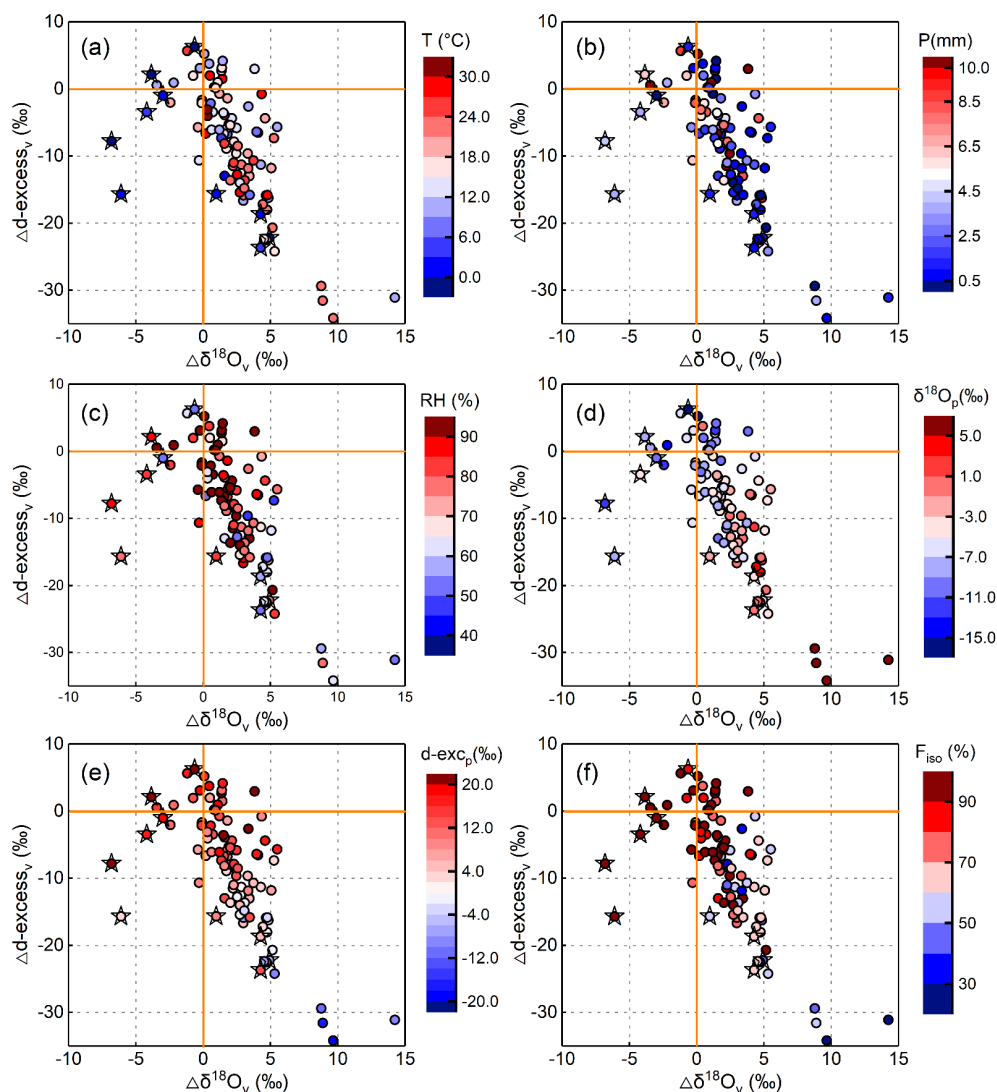
523   Figure 5 $\triangle d \triangle \delta$-diagram for the precipitation samples with meteorological factors and
524   precipitation isotopic information. Temperature (a); Precipitation amount (b); Relative humidity
525   (c); $\delta^{18}O_p$ of precipitation (d); d-excess$_p$ of precipitation (e); Remaining fraction of evaporation
526   (f). The dots with a star represent the snow samples.

527

528   In contrast to meteorological factors, the pattern of precipitation isotopic composition

529   distribution on the $\triangle d \triangle \delta$-diagram is more clear. Under the high below-cloud

530   evaporation condition, the $\delta^{18}O_p$ is more positive and d-excess$_p$ is relatively negative

531   (Fig. 5d and 5e). Correspondingly, the differences between equilibrated $\delta^{18}O_{eq-v}$, d-

532   excess$_{eq-v}$ and observed $\delta^{18}O_{gr-v}$, d-excess$_{gr-v}$ are larger. Conversely, under low below-

Atmospheric
Chemistry
and Physics
Discussions
Open Access
EGU

533 cloud evaporation conditions, mainly corresponding to the most snow samples, we

534 could see the lowest $\delta^{18}O_p$ and highest d-excess$_p$ samples, respectively (Fig. 5d and

535 5e). Moreover, the $\triangle^{18}O_v$ is lower than 0‰ and $\triangle$d-excess$_v$ is placed around 0‰.

536 Basically, the $\triangle$d$\triangle\delta$-diagram follows the traditional explanation, and provides more

537 information, such as the cloud signals, equilibrium conditions, to the falling raindrops.

538

539 By contrast, the slope of the regression line of $\triangle$d/$\triangle\delta$ is -1.9 in our study (Fig. 4),

540 which is more negative than result shown by Graf's et al. (2019). According to the

541 sensitivity test by Graf et al. (2019), RH has a considerable impact on the slope of $\triangle$

542 d/$\triangle$ δ. As our sampling site is located in a semi-arid area and Graf's et al. (2019)

543 location is in the zone of a temperate marine climate, the different slope in two sites

544 may be caused by the differences in RH. Therefore, the $\triangle$d/$\triangle\delta$ slope of -1.9 is

545 possible to be related to the arid or semi-arid conditions, and $\triangle$d/$\triangle\delta$ slope of -0.3

546 could represent a general characteristic of rainfall for continental mid-latitude cold front

547 passages. Certainly, to explore the relationship between the slope of $\triangle$d/$\triangle\delta$ and the

548 climatic characteristic, more validation works need to be done in the future studies.

549

550 **3.3 Comparing and analyzing the differences between F_{iso} and $F_{raindrop}$**

551 **3.3.1 The differences and reasons**

552 In 1975, Stewart (1975) presented a set of empirical models, which is still widely used,

553 to evaluate the below-cloud evaporation rate of the falling raindrop. However, being

554 limited by measuring the cloud-based isotopic composition of the raindrop, many

555 studies turn to use mass conservation model to evaluate the evaporation rate of the

556 raindrop during its falling (Kong et al., 2013; Li et al., 2016a; Sun et al., 2020; Wang et

557 al., 2016b). Here, to compare their differences, we used the isotopic method and mass

558 conservation model, respectively, to calculate the F_r after the below-cloud evaporation.

559

560 As shown in Fig. 6a, the mean of computed reaming fraction is 76.3% by the isotopic

561 method (F_{iso}), and 65.6% by the mass conservation model ($F_{raindrop}$) based on two-year

562 statistical results. The $F_{raindrop}$ is statistically lower than the F_{iso} depending on the

563 independent t-test (F=1.49, p<0.01). In addition, the F_{iso} and $F_{raindrop}$ show an obvious

564 difference, the F_{iso} and $F_{raindrop}$ deviating from 1:1 line, when the F_{iso} equals to 60%~80%

565 (Fig. 6b). On a seasonal scale, the difference between F_{iso} and $F_{raindrop}$ in spring,

566 summer, autumn, winter is 13.7%, 12.8%, 6.0%, and 25.0%, respectively, which is the

567   largest in winter, and the lowest in autumn (Fig. 7).
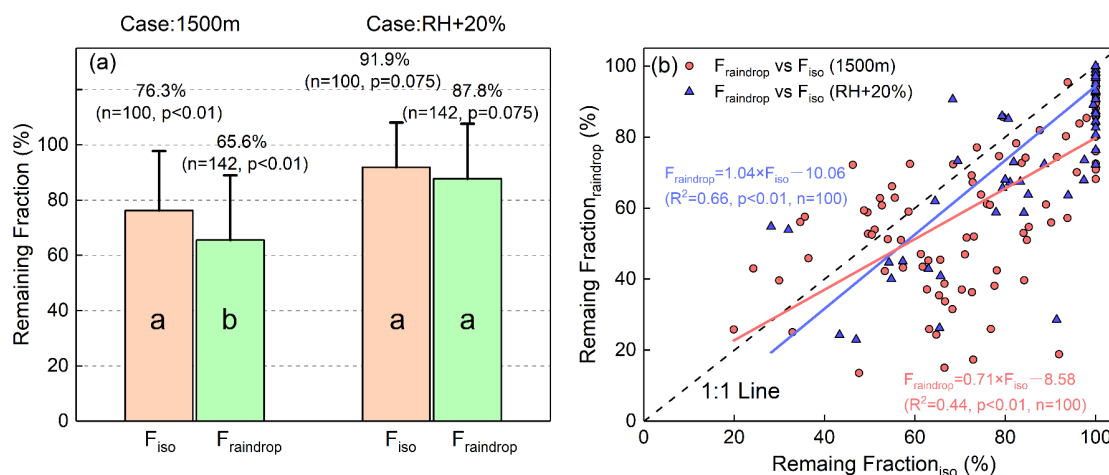
568   Figure 6 The comparison between the remaining fraction calculated by two methods. In (a), the
569   taupe bars and the abbreviation of F_{iso} represent the remaining fraction calculated by the
570   isotopic method, and the green bars and the abbreviation of $F_{raindrop}$ represent the remaining
571   fraction calculated by the mass conservation method. Case 1500m denotes that the raindrops
572   evaporation calculation is based on the assumption of the cloud base at 1500m, and the
573   raindrops are formed at that altitude. Case RH+20% denotes that based on the condition of
574   case 1500m, we calculated the remaining fraction by increasing the ground observed RH by
575   20%. n represents the number of samples used in statistics. The a and b in the bars denote the
576   results of the independent t-test. In (b), the red dots represent the computed results of the
577   remaining fraction under case 1500m condition, and the blue triangles represent the computed
578   results under case RH+20% condition. The dash line is the 1:1 line.
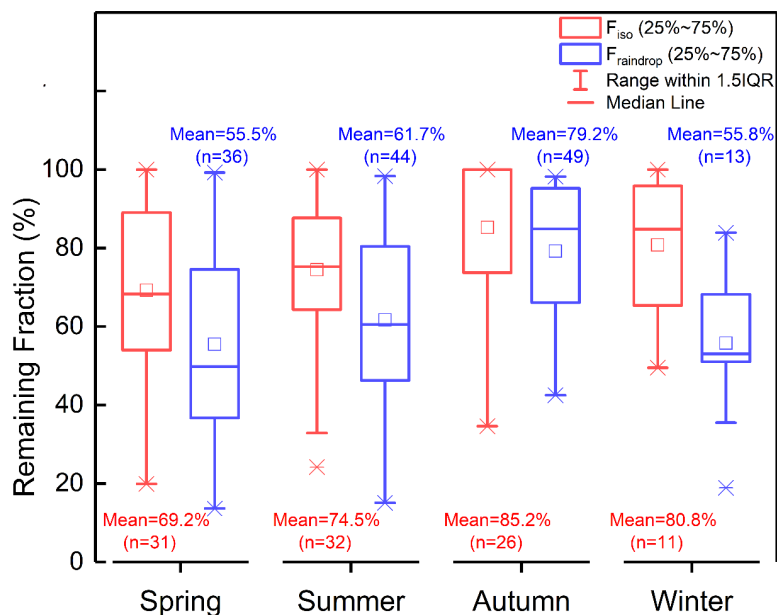
579

580

581

582

583

584

585

586

587

588

589

590

591

592

602 Figure 7 Comparison between the mean remaining fraction results calculated by two methods
603 in four seasons. n represent the number of samples used in statistics.

604

605 To further explore the reason for the large differences by employing different methods,

606 we performed the correlation analyses between meteorological factors and the

607 remaining fraction of evaporation (Fig. S2). These analyses reveal that the most

608 important impact factor both on F_{iso} and $F_{raindrop}$ is RH (Fig. S2b). Although precipitation

609 amount influences F_{iso} and $F_{raindrop}$ as well, their relationship is non-linear, and its effect

610 on F_{iso} is rather weak ($R^2=0.16$, Fig. S2c). For temperature, no clear correlation was

611 found. Wang et al. (2016b) explicitly pointed that among the parameters of temperature,

612 precipitation amount, RH, and raindrop diameter, RH generally plays a decisive role

613 on the obtained $\triangle$d-excess, which is positively correlated with the remaining fraction

614 of raindrop.

615

616 In order to analyze the underlying reason, first, we checked the equation used to

617 calculate F_{iso} and $F_{raindrop}$. We noted that in both methods, RH is an important parameter

618 to compute the remaining ratio. In the equation for computing F_{iso}, the values of γ and

619 β are highly dependent on RH. Equally, in the $F_{raindrop}$ computing equation, RH will be

620 the decisive factor of evaporation intensity (E). Then, we tested the sensitivity between

621 $\triangle\delta^{18}O$ and RH under different F_{iso} levels (Fig. S3). Our results showed, under high RH

622 condition (60%~90%), a little variation of $\triangle\delta^{18}O$ corresponded to a wide range of F_{iso}

623 distribution. We also noticed, under higher RH condition (above 90%), the simulated

624 $\triangle \delta^{18}O$ is very small, normally lower than 0.5‰. However, in reality, the $\triangle \delta^{18}O$ is

625 generally greater than 0.5‰. Therefore, when the actual $\triangle \delta^{18}O$ value is larger than

626 the theoretical value, the calculated F_{iso} results will be larger than 100%, and this is in

627 accordance with the actual condition. Because under higher RH condition, the raindrop

628 evaporation ratio will decrease, and in turn the F_r will appropriately increase. Moreover,

629 in the near-saturated air column, the raindrop is hardly evaporated.

630

631 Therefore, it is reasonable to assume that when the RH is higher, the difference

632 between the F_{iso} and $F_{raindrop}$ will be reduced. To validate our assumption, we computed

633 the F_{iso} and $F_{raindrop}$ by increasing RH by 20%, respectively. As expected, the mean

634 annual difference was highly reduced, and statistically there is no significant difference

635 (Fig. 6a, independent t-test, F=5.665, p=0.075). Moreover, the F_r computed by those

636 two methods is closer to each other, while the correlation coefficient is highly increased,

637 and the slope is closer to 1 (Fig. 6b). For the seasonal variations of F_r, the larger

638 differences between F_{iso} and $F_{raindrop}$ in spring and summer are regarding to the low RH

639 in these seasons, while the small difference in autumn is related to the higher RH. For

640 the largest difference in winter, it is most likely due to the fact that in the mass

641 conservation model, the diameter of raindrop used to determine the terminal velocity

642 of the raindrop (v_{end}) and the evaporation intensity (E) do not take snowfall factor into

643 account resulting a great uncertainty in the calculation results.

644

645 **3.3.2 Sensitivity test**

646 In the below-cloud isotopic evaporation model (eq. 7), the two controlling factors are

647 the equilibrium fractionation factor (α) and the RH. As the equilibrium fractionation

648 factor varies with the cloud base altitude (mainly caused by the variation of

649 temperature), we used the different altitudes to represent the variations of α. In order

650 to assess the relevance of different ambient conditions for the raindrop evaporation, a

651 sensitivity test of F_r under different altitude and RH scenarios is exhibited in Fig. S4.

652 With the increase of altitude, the F_r is gradually decreased. It is well known that with

653 the increase of altitude, the raindrop falling distance will increase, and correspondingly

654 the falling time will be extended. As a result, more fraction of raindrops would be

655 evaporated in the unsaturated atmospheric columns. When the RH increases by 20%,

656 the atmospheric columns is near saturated, and largely decrease the evaporation

657 possibility of falling raindrops. Conversely, the decrease of RH will strongly increase

658 the evaporation proportion of falling raindrops. In addition, according to Fig. S4, the F_r

659   seems to be more sensitive to the changing of RH than that of altitude.

660

661   Overall, in our study, the mass conservation method will overestimate the raindrop

662   evaporation ratios relative to the isotopic method. The overestimation may be related

663   to the low RH in our studying location. If we increase the RH by 20%, there is no

664   significant difference between the two methods. This indicates that in high RH areas,

665   either method could be used to calculate the F_r. However, in those arid and semi-arid

666   areas, where the RH is relatively low, and the high latitude regions, where snowfall is

667   frequent in winter, we need to cautiously use the result computed by the mass

668   conservation method. In the future, it will be promising to study the raindrop formation

669   height and upper atmospheric water vapor isotopic composition when considering the

670   below-cloud processes of raindrop.

671

672   **3.4 The characteristics of below-cloud evaporation of raindrop in Xi'an**

673   As the phenomenon of below-cloud evaporation is very common in arid and semi-arid

674   regions, to explore the information contained in the precipitation isotopic composition,

675   it is important to clearly know that how much of the raindrops have been evaporated

676   before they land on the ground. Here, we summarized the seasonal variations of F_{iso}

677   in Xi'an (Fig. 8).
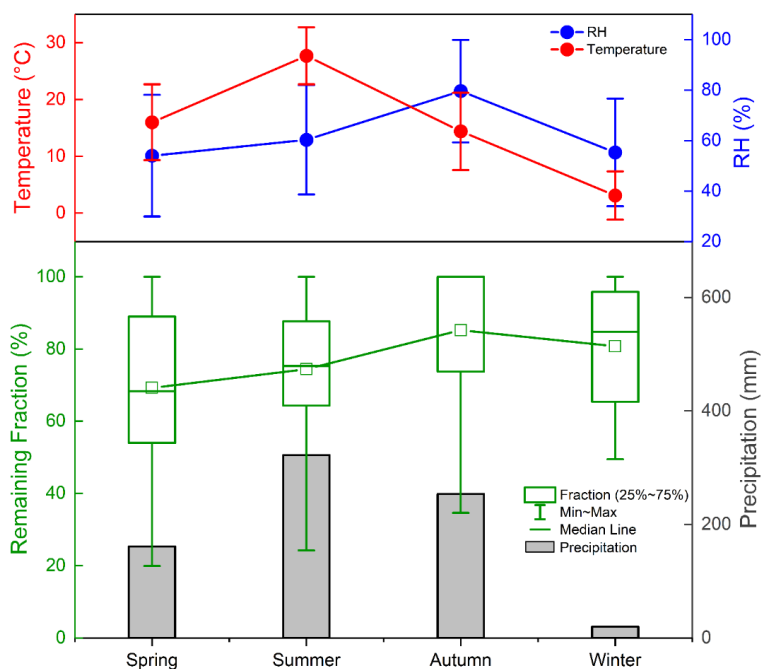
Atmospheric
Chemistry
and Physics
Discussions

Open Access

EGU

695 Figure 8 The variations of temperature, relative humidity, precipitation amount and mean

696 remaining fraction of evaporated raindrops in four seasons in Xi'an

697

698 By seasonally dividing the precipitation isotopic composition on the $\triangle d \triangle \delta$-diagram, it

699 showed that samples collected in spring and summer dominate the evaporation phase,

700 reflecting a stronger evaporation influence, while most of the winter precipitation and

701 part of autumn precipitation monopolize the cloud signal phase indicating a weak or

702 no below-cloud evaporation on these samples (Fig. S5). In addition, part of the autumn

703 samples, in which the below-cloud evaporation and cloud-based isotopic exchange

704 tends to achieve a complete equilibrium state is distributed in the equilibration phase

705 (Fig. S5). Moreover, the raindrops F_{iso} distribution on the $\triangle d \triangle \delta$-diagram is also

706 related to the below-cloud processes (Fig. 5f).

707

708 The mean raindrop evaporation rate is highest in spring and lowest in autumn based

709 on two-year data (Fig. 8). The seasonal variation of F_{iso} basically followed the trend of

710 seasonal variation of RH. Although the precipitation amount is highest in the summer,

711 the temperature is extremely high and RH is relatively low, which causes the high

712 evaporation rate in summer. In winter, the low evaporation rate may be related to the

713 precipitation type, because snowfall is the main deposition type in this season.

714

715 **4 Conclusions**

716 The below-cloud processes acting on precipitation are complex and changeable,

717 especially in the arid and semi-arid regions. Previously, using the slope of LMWL and

718 d-excess of precipitation, we can only speculate the raindrops experienced below-

719 cloud processes according to the relative change of precipitation isotopic composition.

720 However, to display our data on the $\triangle d \triangle \delta$-diagram, which is suggested by Graf et al.

721 (2019), we can more intuitively determine the happened below-cloud processes on the

722 falling raindrops. The $\triangle d \triangle \delta$-diagram provides a new tool for us to qualitatively realize

723 the below-cloud processes of raindrops.

724

725 In this study, based on the two-year precipitation data collected in Xi'an, we

726 systematically analyze its below-cloud processes, and get the following main

727 conclusions:

728 1. In Xi'an, the precipitation isotopic signals mainly record the information of water

729 vapor isotopic composition, but the signals could be altered by the below-cloud

730 evaporation effect. This remind us to be cautious to study the hydrological cycle and

731   climate changes by using precipitation isotopic signals in the arid and semi-arid regions.

732   2. Our work validates the general applicability of the $\triangle$d$\triangle$δ-diagram. According to $\triangle$d

733    $\triangle$δ-diagram, the below-cloud evaporation is the main process during the raindrops

734   falling. For the snowfall samples, they are less influenced by the below-cloud

735   processes, and preserve its initial water vapor information. Hence, our results further

736   strengthen the reliability by using ice-core to reconstruct the paleoclimate,

737   paleoenvironment, and paleohydrology in the cold area. The different $\triangle$d/$\triangle$δ slopes

738   in our work and Graf's et al. (2019) study may represent the different climate conditions,

739   and it will be more convincible to explore the slope for more climatic regions in future

740   studies.

741   3. Compared with the isotopic method, the evaporation rate computed by the mass

742   conservation model is overestimated. Relative humidity is the main controlling factor

743   in computing the remaining fraction of raindrops below-cloud evaporation. Due to more

744   undeterminable parameters in the mass conservation model, such as raindrop

745   diameter, evaporation intensity, raindrop falling velocity, and no consideration of

746   precipitation type, it is more suitable to use isotopic model to calculate the remaining

747   fraction of evaporated raindrops.

748   4. In the semi-arid city of CLP, the evaporation rates are higher in spring and summer,

749   and lower in autumn and winter, and this is related to the variation of local RH.

Data availability

The datasets can be obtained from the TableS1.

Author contribution

Meng Xing and Weiguo Liu designed the experiments, interpreted the results, and
prepared the manuscript with contributions from all co-authors. Meng Xing and Jing
Hu analyzed the precipitation and water vapor samples. Jing Hu maintained the
experimental instruments.

Competing interests

The authors declare that they have no conflict of interest.

Atmospheric
Chemistry
and Physics
Discussions

References

Aemisegger, F., Sturm, P., Graf, P., Sodemann, H., Pfahl, S., Knohl, A. and Wernli, H.: Measuring variations of δ 18O and δ 2H in atmospheric water vapour using two commercial laser-based spectrometers: An instrument characterisation study, Atmos. Meas. Tech., 5(7), 1491–1511, doi:10.5194/amt-5-1491-2012, 2012.

Aemisegger, F., Spiegel, J. K., Pfahl, S., Sodemann, H., Eugster, W. and Wernli, H.: Isotope meteorology of cold front passages: A case study combining observations and modeling, Geophys. Res. Lett., 42(13), 5652–5660, doi:10.1002/2015GL063988, 2015.

Bastrikov, V., Steen-Larsen, H. C., Masson-Delmotte, V., Gribanov, K., Cattani, O., Jouzel, J. and Zakharov, V.: Continuous measurements of atmospheric water vapour isotopes in western Siberia (Kourovka), Atmos. Meas. Tech., 7(6), 1763–1776, doi:10.5194/amt-7-1763-2014, 2014.

Benetti, M., Reverdin, G., Pierre, C., Merlivat, L., Risi, C., Steen-Larsen, H. C. and Vimeux, F.: Deuterium excess in marine water vapor: Dependency on relative humidity and surface wind speed during evaporation, J. Geophys. Res., 119(2), 584–593, doi:10.1002/2013JD020535, 2014.

Bowen, G. J., Cai, Z., Fiorella, R. P. and Putman, A. L.: Isotopes in the Water Cycle: Regional-to Global-Scale Patterns and Applications, Annu. Rev. Earth Planet. Sci., 47(1), 453–479, doi:10.1146/annurev-earth-053018-060220, 2019.

Cai, Y., Cheng, H., An, Z., Edwards, R. L., Wang, X., Tan, L. and Wang, J.: Large variations of oxygen isotopes in precipitation over south-central Tibet during Marine Isotope Stage 5, Geology, 38(3), 243–246, doi:10.1130/G30306.1, 2010.

Chakraborty, S., Sinha, N., Chattopadhyay, R., Sengupta, S., Mohan, P. M. and Datye, A.: Atmospheric controls on the precipitation isotopes over the Andaman Islands, Bay of Bengal, Sci. Rep., 6, 19555 [online] Available from: https://doi.org/10.1038/srep19555, 2016.

Christner, E., Aemisegger, F., Pfahl, S., Werner, M., Cauquoin, A., Schneider, M., Hase, F., Barthlott, S. and Schädler, G.: The Climatological Impacts of Continental Surface Evaporation, Rainout, and Subcloud Processes on δD of Water Vapor and Precipitation in Europe, J. Geophys. Res. Atmos., 123(8), 4390–4409, doi:10.1002/2017JD027260, 2018.

Clark, I. D. and Fritz, P.: Environmental Isotopes in Hydrogeology, Lewis, Boca Raton, Florida., 1997.

804   Craig, H.: Isotopic Variations in Meteoric Waters, Science (80-.)., 133(3465), 1702–1703, 1961.

805   Crosson, E. R.: A cavity ring-down analyzer for measuring atmospheric levels of methane,
806   carbon dioxide, and water vapor, Appl. Phys. B, 92(3), 403–408, doi:10.1007/s00340-008-
807   3135-y, 2008.

808   Dansgaard, W.: Stable isotopes in precipitation, Tellus, 16(4), 436–468,
809   doi:10.3402/tellusa.v16i4.8993, 1964.

810   Deshpande, R. D., Maurya, A. S., Kumar, B., Sarkar, A. and Gupta, S. K.: Rain-vapor
811   interaction and vapor source identification using stable isotopes from semiarid western India, J.
812   Geophys. Res. Atmos., 115(23), 1–11, doi:10.1029/2010JD014458, 2010.

813   Ellehoj, M. D., Steen-Larsen, H. C., Johnsen, S. J. and Madsen, M. B.: Ice-vapor equilibrium
814   fractionation factor of hydrogen and oxygen isotopes: experimental investigations and
815   implications for stable water isotope studies, Rapid Commun. Mass Spectrom. Rcm, 27(19),
816   2149–2158, 2013.

817   Fiorella, R. P., Bares, R., Lin, J. C., Ehleringer, J. R. and Bowen, G. J.: Detection and variability
818   of combustion-derived vapor in an urban basin, Atmos. Chem. Phys., 18(12), 8529–8547,
819   doi:10.5194/acp-18-8529-2018, 2018.

820   Froehlich, K., Kralik, M., Papesch, W., Rank, D., Scheifinger, H. and Stichler, W.: Deuterium
821   excess in precipitation of Alpine regions – moisture recycling, Isotopes Environ. Health Stud.,
822   44(1), 61–70, doi:10.1080/10256010801887208, 2008.

823   Gat, J. R.: OXYGEN AND HYDROGEN ISOTOPES IN THE HYDROLOGIC CYCLE, Annu.
824   Rev. Earth Planet. Sci., 24(1), 225–262, doi:10.1146/annurev.earth.24.1.225, 1996.

825   Gorski, G., Strong, C., Good, S. P., Bares, R., Ehleringer, J. R. and Bowen, G. J.: Vapor
826   hydrogen and oxygen isotopes reflect water of combustion in the urban atmosphere, Proc. Natl.
827   Acad. Sci., 112(11), 3247–3252, doi:10.1073/pnas.1424728112, 2015.

828   Graf, P., Wernli, H., Pfahl, S. and Sodemann, H.: A new interpretative framework for below-
829   cloud effects on stable water isotopes in vapour and rain, Atmos. Chem. Phys., 19(2), 747–765,
830   doi:10.5194/acp-19-747-2019, 2019.

831   Griffis, T. J., Wood, J. D., Baker, J. M., Lee, X., Xiao, K., Chen, Z., Welp, L. R., Schultz, N. M.,
832   Gorski, G., Chen, M. and Nieber, J.: Investigating the source, transport, and isotope
833   composition of water vapor in the planetary boundary layer, Atmos. Chem. Phys., 16(8), 5139–
834   5157, doi:10.5194/acp-16-5139-2016, 2016.

835   Gupta, P., Noone, D., Galewsky, J., Sweeney, C. and Vaughn, B. H.: Demonstration of high-
836   precision continuous measurements of water vapor isotopologues in laboratory and remote
837   field deployments using wavelength-scanned cavity ring-down spectroscopy (WS-CRDS)
838   technology, Rapid Commun Mass Spectrom, 23(16), 2009.

839   Horita, J. and Wesolowski, D. J.: Liquid-vapor fractionation of oxygen and hydrogen isotopes
840   of water from the freezing to the critical temperature, Geochim. Cosmochim. Acta, 58(16),
841   3425–3437, 1994.

842   Jacob, H. and Sonntag, C.: An 8-year record of the seasonal variation of 2 H and 18 O in
843   atmospheric water vapour and precipitation at Heidelberg, Germany, Tellus B Chem. Phys.

844 Meteorol., 43(3), 291–300, doi:10.3402/tellusb.v43i3.15276, 1991.

845 Jeelani, G., Deshpande, R. D., Galkowski, M. and Rozanski, K.: Isotopic composition of daily

846 precipitation along the southern foothills of the Himalayas: Impact of marine and continental

847 sources of atmospheric moisture, Atmos. Chem. Phys., 18(12), 8789–8805, doi:10.5194/acp-

848 18-8789-2018, 2018.

849 Kong, Y., Pang, Z. and Froehlich, K.: Quantifying recycled moisture fraction in precipitation of

850 an arid region using deuterium excess . Tellus Series B Chem Phys Meteorol Quantifying

851 recycled moisture fraction in precipitation of an arid region using deuterium excess, Tellus B,

852 65(August 2015), 1–8, doi:10.3402/tellusb.v65i0.19251, 2013.

853 Laskar, A. H., Huang, J. C., Hsu, S. C., Bhattacharya, S. K., Wang, C. H. and Liang, M. C.:

854 Stable isotopic composition of near surface atmospheric water vapor and rain-vapor interaction

855 in Taipei, Taiwan, J. Hydrol., 519(PB), 2091–2100, doi:10.1016/j.jhydrol.2014.10.017, 2014.

856 Li, L. and Garzione, C. N.: Spatial distribution and controlling factors of stable isotopes in

857 meteoric waters on the Tibetan Plateau : Implications for paleoelevation reconstruction, Earth

858 Planet. Sci. Lett., 460, 302–314, doi:10.1016/j.epsl.2016.11.046, 2017.

859 Li, Z., Qi, F., Wang, Q. J., Kong, Y., Cheng, A., Song, Y., Li, Y., Li, J. and Guo, X.: Contributions

860 of local terrestrial evaporation and transpiration to precipitation using δ 18 O and D-excess as

861 a proxy in Shiyang inland river basin in China, Glob. Planet. Chang., 146, 140–151, 2016a.

862 Li, Z., Feng, Q., Wang, Y., Li, J., Guo, X. and Li, Y.: Effect of sub-cloud evaporation on the δ

863 18 O of precipitation in Qilian Mountains and Hexi Corridor , China, Sci. Cold Arid Reg., 8(5),

864 378–387, doi:10.3724/SP.J.1226.2016.00378.Effect, 2016b.

865 Liu, W., Feng, X., Liu, Y., Zhang, Q. and An, Z.: δ18O values of tree rings as a proxy of monsoon

866 precipitation in arid Northwest China, Chem. Geol., 206(1), 73–80,

867 doi:https://doi.org/10.1016/j.chemgeo.2004.01.010, 2004.

868 Liu, W., Liu, H., Wang, Z., An, Z. and Cao, Y.: Hydrogen isotopic compositions of long-chain

869 leaf wax n-alkanes in Lake Qinghai sediments record palaeohydrological variations during the

870 past 12 ka, Quat. Int., 449, 67–74, doi:https://doi.org/10.1016/j.quaint.2017.05.024, 2017a.

871 Liu, W., Wang, H., Leng, Q., Liu, H., Zhang, H. and Xing, M.: Hydrogen isotopic compositions

872 along a precipitation gradient of Chinese Loess Plateau : Critical roles of precipitation /

873 evaporation and vegetation change as controls for leaf wax δ D, Chem. Geol., 528(April),

874 119278, doi:10.1016/j.chemgeo.2019.119278, 2019.

875 Liu, Y., Liu, H., Song, H., Li, Q., Burr, G. S., Wang, L. and Hu, S.: A monsoon-related 174-year

876 relative humidity record from tree-ring δ18O in the Yaoshan region, eastern central China, Sci.

877 Total Environ., 593–594, 523–534, doi:https://doi.org/10.1016/j.scitotenv.2017.03.198, 2017b.

878 Ma, Q., Zhang, M., Wang, S., Wang, Q., Liu, W., Li, F. and Chen, F.: An investigation of

879 moisture sources and secondary evaporation in Lanzhou, Northwest China, Environ. Earth Sci.,

880 71(8), 3375–3385, doi:10.1007/s12665-013-2728-x, 2014.

881 Müller, S., Stumpp, C., Sørensen, J. H. and Jessen, S.: Spatiotemporal variation of stable

882 isotopic composition in precipitation: Post-condensational effects in a humid area, Hydrol.

883 Process., 31(18), 3146–3159, doi:10.1002/hyp.11186, 2017.

884 Noone, D., Galewsky, J., Sharp, Z. D., Worden, J., Barnes, J., Baer, D., Bailey, A., Brown, D.
885 P., Christensen, L., Crosson, E., Dong, F., Hurley, J. V., Johnson, L. R., Strong, M., Toohey,
886 D., Van Pelt, A. and Wright, J. S.: Properties of air mass mixing and humidity in the subtropics
887 from measurements of the D/H isotope ratio of water vapor at the Mauna Loa Observatory, J.
888 Geophys. Res. Atmos., 116(22), 1–18, doi:10.1029/2011JD015773, 2011.

889 Noone, D., Risi, C., Bailey, A., Berkelhammer, M., Brown, D. P., Buenning, N., Gregory, S.,
890 Nusbaumer, J., Schneider, D., Sykes, J., Vanderwende, B., Wong, J., Meillier, Y. and Wolfe,
891 D.: Determining water sources in the boundary layer from tall tower profiles of water vapor and
892 surface water isotope ratios after a snowstorm in Colorado, Atmos. Chem. Phys., 13(3), 1607–
893 1623, doi:10.5194/acp-13-1607-2013, 2013.

894 Peng, H., Mayer, B., Harris, S. and Krouse, H. R.: The influence of below-cloud secondary
895 effects on the stable isotope composition of hydrogen and oxygen in precipitation at Calgary,
896 Alberta, Canada, Tellus, Ser. B Chem. Phys. Meteorol., 59(4), 698–704, doi:10.1111/j.1600-
897 0889.2007.00291.x, 2007.

898 Peng, T. R., Liu, K. K., Wang, C. H. and Chuang, K. H.: A water isotope approach to assessing
899 moisture recycling in the island-based precipitation of Taiwan: A case study in the western
900 Pacific, Water Resour. Res., 47(8), 1–11, doi:10.1029/2010WR009890, 2011.

901 Putman, A. L., Fiorella, R. P., Bowen, G. J. and Cai, Z.: A Global Perspective on Local Meteoric
902 Water Lines: Meta-analytic Insight into Fundamental Controls and Practical Constraints, Water
903 Resour. Res., 2019WR025181, doi:10.1029/2019WR025181, 2019.

904 Rangarajan, R., Laskar, A. H., Bhattacharya, S. K., Shen, C. C. and Liang, M. C.: An insight
905 into the western Pacific wintertime moisture sources using dual water vapor isotopes, J. Hydrol.,
906 547, 111–123, doi:10.1016/j.jhydrol.2017.01.047, 2017.

907 Salamalikis, V., Argiriou, A. A. and Dotsika, E.: Isotopic modeling of the sub-cloud evaporation
908 effect in precipitation, Sci. Total Environ., 544, 1059–1072, doi:10.1016/j.scitotenv.2015.11.072,
909 2016.

910 Salmon, O. E., Welp, L. R., Baldwin, M., Hajny, K., Stirm, B. H. and Shepson, P. B.: Vertical
911 profile observations of water vapor deuterium excess in the lower troposphere, Atmos. Chem.
912 Phys. Discuss., (January), 1–35, doi:10.5194/acp-2018-1313, 2019.

913 Steen-Larsen, H. C., Johnsen, S. J., Masson-Delmotte, V., Stenni, B., Risi, C., Sodemann, H.,
914 Balslev-Clausen, D., Blunier, T., Dahl-Jensen, D., Ellehøj, M. D., Falourd, S., Grindsted, A.,
915 Gkinis, V., Jouzel, J., Popp, T., Sheldon, S., Simonsen, S. B., Sjolte, J., Steffensen, J. P.,
916 Sperlich, P., Sveinbjörnsdóttir, A. E., Vinther, B. M. and White, J. W. C.: Continuous monitoring
917 of summer surface water vapor isotopic composition above the Greenland Ice Sheet, Atmos.
918 Chem. Phys., 13(9), 4815–4828, doi:10.5194/acp-13-4815-2013, 2013.

919 Steen-Larsen, H. C., Masson-Delmotte, V., Hirabayashi, M., Winkler, R., Satow, K., Prié, F.,
920 Bayou, N., Brun, E., Cuffey, K. M., Dahl-Jensen, D., Dumont, M., Guillevic, M., Kipfstuhl, S.,
921 Landais, A., Popp, T., Risi, C., Steffen, K., Stenni, B. and Sveinbjörnsdottír, A. E.: What controls
922 the isotopic composition of Greenland surface snow?, Clim. Past, 10(1), 377–392,
923 doi:10.5194/cp-10-377-2014, 2014.

924 Stewart, M. K.: Stable isotope fractionation due to evaporation and isotopic exchange of falling
925 waterdrops: Applications to atmospheric processes and evaporation of lakes, J. Geophys. Res.,
926 80(9), 1133–1146, doi:10.1029/JC080i009p01133, 1975.

927 Sun, C., Chen, Y., Li, J., Chen, W. and Li, X.: Stable isotope variations in precipitation in the
928 northwesternmost Tibetan Plateau related to various meteorological controlling factors, Atmos.
929 Res., 227(April), 66–78, doi:10.1016/j.atmosres.2019.04.026, 2019.

930 Sun, C., Chen, W., Chen, Y. and Cai, Z.: Stable isotopes of atmospheric precipitation and its
931 environmental drivers in the Eastern Chinese Loess Plateau , China, J. Hydrol., 581(November
932 2019), 124404, doi:10.1016/j.jhydrol.2019.124404, 2020.

933 Tan, L., An, Z., Huh, C.-A., Cai, Y., Shen, C.-C., Shiau, L.-J., Yan, L., Cheng, H. and Edwards,
934 R. L.: Cyclic precipitation variation on the western Loess Plateau of China during the past four
935 centuries, Sci. Rep., 4(1), 6381, doi:10.1038/srep06381, 2014.

936 Thompson, L. G., Yao, T., Mosley-Thompson, E., Davis, M. E., Henderson, K. A. and Lin, P.-
937 N.: A High-Resolution Millennial Record of the South Asian Monsoon from Himalayan Ice Cores,
938 Science (80-.)., 289(5486), 1916 LP – 1919, doi:10.1126/science.289.5486.1916, 2000.

939 Tian, C., Wang, L., Kaseke, K. F. and Bird, B. W.: Stable isotope compositions (δ 2 H , δ 18 O
940 and δ 17 O) of rainfall and snowfall in the central United States, Sci. Rep., (October 2017), 1–
941 15, doi:10.1038/s41598-018-25102-7, 2018.

942 Wan, H., Liu, W. and Xing, M.: Isotopic composition of atmospheric precipitation and its tracing
943 significance in the Laohequ Basin, Loess plateau, China, Sci. Total Environ., 640–641(May),
944 989–996, doi:10.1016/j.scitotenv.2018.05.338, 2018.

945 Wang, S., Zhang, M., Che, Y., Chen, F. and Fang, Q.: Contribution of recycled moisture to
946 precipitation in oases of arid central Asia: A stable isotope approach, Water Resour. Res., 52(4),
947 3246–3257, doi:10.1002/2015WR018135, 2016a.

948 Wang, S., Zhang, M., Che, Y., Zhu, X. and Liu, X.: Influence of Below-Cloud Evaporation on
949 Deuterium Excess in Precipitation of Arid Central Asia and Its Meteorological Controls, J.
950 Hydrometeorol., 17(7), 1973–1984, doi:10.1175/JHM-D-15-0203.1, 2016b.

951 Wang, S., Zhang, M., Hughes, C. E., Crawford, J., Wang, G., Chen, F., Du, M., Qiu, X. and
952 Zhou, S.: Meteoric water lines in arid Central Asia using event-based and monthly data, J.
953 Hydrol., 562(May), 435–445, doi:10.1016/j.jhydrol.2018.05.034, 2018a.

954 Wang, Z., An, Z., Liu, Z., Qiang, X., Zhang, F. and Liu, W.: Hydroclimatic variability in loess
955 δDwax records from the central Chinese Loess Plateau over the past 250 ka, J. Asian Earth
956 Sci., 155, 49–57, doi:https://doi.org/10.1016/j.jseaes.2017.11.008, 2018b.

957 Welp, L. R., Lee, X., Kim, K., Griffis, T. J., Billmark, K. A. and Baker, J. M.: δ18O of water
958 vapour, evapotranspiration and the sites of leaf water evaporation in a soybean canopy, Plant,
959 Cell Environ., 31(9), 1214–1228, doi:10.1111/j.1365-3040.2008.01826.x, 2008.

960 Welp, L. R., Lee, X., Griffis, T. J., Wen, X. F., Xiao, W., Li, S., Sun, X., Hu, Z., Val Martin, M.
961 and Huang, J.: A meta-analysis of water vapor deuterium-excess in the midlatitude atmospheric
962 surface layer, Global Biogeochem. Cycles, 26(3), 1–12, doi:10.1029/2011GB004246, 2012.

963 Wen, X., Yang, B., Sun, X. and Lee, X.: Evapotranspiration partitioning through in-situ oxygen

964   isotope measurements in an oasis cropland, Agric. For. Meteorol., 230–231, 89–96,
965   doi:10.1016/j.agrformet.2015.12.003, 2016.

966   Wen, X. F., Zhang, S. C., Sun, X. M., Yu, G. R. and Lee, X.: Water vapor and precipitation
967   isotope ratios in Beijing, China, J. Geophys. Res. Atmos., 115(1), 1–10,
968   doi:10.1029/2009JD012408, 2010.

969   Yao, T., Thompson, L. G., Mosley-Thompson, E., Zhihong, Y., Xingping, Z. and Lin, P.-N.:
970   Climatological significance of δ18O in north Tibetan ice cores, J. Geophys. Res. Atmos.,
971   101(D23), 29531–29537, doi:10.1029/96JD02683, 1996.

972   Yao, T., Masson-Delmotte, V., Gao, J., Yu, W., Yang, X., Risi, C., Sturm, C., Werner, M., Zhao,
973   H., He, Y., Ren, W., Tian, L., Shi, C. and Hou, S.: A review of climatic controls on δ18O in
974   precipitation over the Tibetan Plateau: Observations and simulations, Rev. Geophys., 51(4),
975   525–548, doi:10.1002/rog.20023, 2013.

976   Yu, W., Tian, L., Ma, Y., Xu, B. and Qu, D.: Simultaneous monitoring of stable oxygen isotope
977   composition in water vapour and precipitation over the central Tibetan Plateau, Atmos. Chem.
978   Phys., 15(18), 10251–10262, doi:10.5194/acp-15-10251-2015, 2015.

979   Yu, W., Tian, L., Risi, C., Yao, T., Ma, Y., Zhao, H., Zhu, H., He, Y., Xu, B., Zhang, H. and Qu,
980   D.: δ18O records in water vapor and an ice core from the eastern Pamir Plateau: Implications
981   for paleoclimate reconstructions, Earth Planet. Sci. Lett., 456, 146–156,
982   doi:10.1016/j.epsl.2016.10.001, 2016.

983   Zhang, M. and Wang, S.: A review of precipitation isotope studies in China: Basic pattern and
984   hydrological process, J. Geogr. Sci., 26(7), 921–938 [online] Available from:
985   http://www.geogsci.com, 2016.

986   Zhao, L., Liu, X., Wang, N., Kong, Y., Song, Y., He, Z., Liu, Q. and Wang, L.: Contribution of
987   recycled moisture to local precipitation in the inland Heihe River Basin, Agric. For. Meteorol.,
988   271(July 2018), 316–335, doi:10.1016/j.agrformet.2019.03.014, 2019.

989   Zhu, G. F., Li, J. F., Shi, P. J., He, Y. Q., Cai, A., Tong, H. L., Liu, Y. F. and Yang, L.:
990   Relationship between sub-cloud secondary evaporation and stable isotope in precipitation in
991   different regions of China, Environ. Earth Sci., 75(10), 876, 2016.

992